Biochimica et Biophysica Acta 1852 (2015) 1298–1310

Contents lists available at ScienceDirect

Biochimica et Biophysica Acta

journal homepage: www.elsevier.com/locate/bbadis

Protective effects of resveratrol on the inhibition of hippocampal neurogenesis induced by ethanol during early postnatal life

Le Xu [a,b], Yang Yang [c], Lixiong Gao [d], Jinghui Zhao [a], Yulong Cai [a], Jing Huang [e], Sheng Jing [e], Xiaohang Bao [e], Ying Wang [a], Junwei Gao [a], Haiwei Xu [d,*], Xiaotang Fan [a,*]

[a] Department of Developmental Neuropsychology, School of Psychology, Third Military Medical University, Chongqing 400038, China
[b] The Battalion 5 of Cadet Brigade, Third Military Medical University, Chongqing 400038, China
[c] Department of Neurosurgery, Southwest Hospital, Third Military Medical University, Chongqing 400038, China
[d] Southwest Eye Hospital, Southwest Hospital, Third Military Medical University, 400038, China
[e] Department of Anesthesiology, Xinqiao Hospital, Third Military Medical University, Chongqing 400037, China

ARTICLE INFO

Article history:
Received 31 October 2014
Received in revised form 9 February 2015
Accepted 17 March 2015
Available online 24 March 2015

Keywords:
Ethanol
Neurogenesis
Hippocampal development
Neural precursor cell
Resveratrol

ABSTRACT

Ethanol (EtOH) exposure during early postnatal life triggers obvious neurotoxic effects on the developing hippocampus and results in long-term effects on hippocampal neurogenesis. Resveratrol (RSV) has been demonstrated to exert potential neuroprotective effects by promoting hippocampal neurogenesis. However, the effects of RSV on the EtOH-mediated impairment of hippocampal neurogenesis remain undetermined. Thus, mice were pretreated with RSV and were later exposed to EtOH to evaluate its protective effects on EtOH-mediated toxicity during hippocampal development. The results indicated that a brief exposure of EtOH on postnatal day 7 resulted in a significant impairment in hippocampal neurogenesis and a depletion of hippocampal neural precursor cells (NPCs). This effect was attenuated by pretreatment with RSV. Furthermore, EtOH exposure resulted in a reduction in spine density on the granular neurons of the dentate gyrus (DG), and the spines exhibited a less mature morphological phenotype characterized by a higher proportion of stubby spines and a lower proportion of mushroom spines. However, RSV treatment effectively reversed these responses. We further confirmed that RSV treatment reversed the EtOH-induced down-regulation of hippocampal pERK and Hes1 protein levels, which may be related to the proliferation and maintenance of NPCs. Furthermore, EtOH exposure in the C17.2 NPCs also diminished cell proliferation and activated apoptosis, which could be reversed by pretreatment of RSV. Overall, our results suggest that RSV pretreatment protects against EtOH-induced defects in neurogenesis in postnatal mice and may thus play a critical role in preventing EtOH-mediated toxicity in the developing hippocampus.

1. Introduction

Heavy exposure of ethanol (EtOH) in utero may cause neurodevelopmental malformations and results in behavioral and mental deficits, known as fetal alcohol syndrome (FAS) [1–3]. The hippocampus is involved in cognitive processes, such as learning and memory, and is also extremely vulnerable to the neurotoxic effects of EtOH exposure [4–6]. EtOH exposure during the brain growth spurt in both humans (the third trimester) and rodents (first 2 weeks after birth) triggers obvious neurotoxic effects in the developing hippocampus, results in long-term effects on hippocampal neurogenesis, and produces behavioral and cognitive deficits in adults [7,8]. For example, binge-like alcohol exposure during the neonatal period (PD4–9) and a single episode of alcohol exposure on postnatal day 7 (PD7) decreases neurogenesis in the adult hippocampus [7,8]. However, the underlying mechanisms of early alcohol exposure that cause dysfunction in hippocampal neurogenesis remain unclear.

The mammalian subgranular zone (SGZ) of the hippocampal dentate gyrus (DG) is endowed with a pool of neural precursor cells (NPCs) that divide and produce granule cells throughout life [9]. A great majority of the granule cells in the rat DG are generated postnatally at the peak of proliferation occurring near the end of the first postnatal week [10]. Therefore, the size of the NPC pool may be an important determinant of lifetime neurogenesis and hippocampal function. EtOH exposure in postnatal mice at P7 reduced the pool of neural stem cells and progenitor cells in the DG [7]. Meanwhile, chronic alcohol exposure in adolescent nonhuman primates has been reported to significantly decrease the proliferating progenitor pool in the hippocampal DG, thus leading to a lasting effect on hippocampus-associated cognitive tasks [11]. Meanwhile, the plasticity of the neonatal hippocampus allows for the prevention of the teratogenic effects of EtOH

* Corresponding authors.
E-mail addresses: haiweixu2001@163.com (H. Xu), fanxiaotang2005@163.com (X. Fan).

http://dx.doi.org/10.1016/j.bbadis.2015.03.009
0925-4439/

exposure at an early stage and may be helpful to prevent the occurrence of lifelong brain damage and cognitive dysfunction [12].

Resveratrol (RSV) is a natural stilbene found in the skin of red grapes and in certain medicinal plants [13,14]. RSV has been shown to display multiple neuroprotective effects [15,16]. Treatment with a single dose of RSV after trauma significantly ameliorates trauma-induced hippocampal neuronal loss in rats [17]. In addition, RSV decreases anxiety and increases cortex- and hippocampus-dependent memories in animals subjected to blunt head trauma [18]. RSV has also been recently reported to promote the survival of adult hippocampal NPCs in an animal model of neuroinflammation [19], whereas another study reported that the hippocampal NPCs of intact mice seem to be adversely affected by RSV [20]. Meanwhile, RSV has been demonstrated to decrease brain injury, including injury in the hippocampus, caused by neonatal hypoxic–ischemic [21], and RSV treatment enhanced the generation of newly born neurons in the DG in prenatally stressed rat brains [22]. However, whether RSV can prevent the EtOH-induced exhaustion of the NPC pool in neonatal mice has not yet been examined.

In the present study, mice were pretreated with RSV and were then exposed to EtOH to evaluate the protective effects of RSV against EtOH-mediated toxicity to hippocampal development. We used 5-bromo-2-deoxyuridine (BrdU) and doublecortin (DCX) to investigate the protection of RSV against EtOH-mediated toxicity of hippocampal neurogenesis. In addition, RSV protection against EtOH induced depletion of the NPC pool in the DG was evaluated by double-immunofluorescently stained with SOX2/GFAP, BLBP/Nestin and GFAP/BLBP. The extracellular signal-regulated protein kinase (ERK1/2) belongs to the MAPK family, and has been shown to be involved in the proliferation of NPCs [23]. Hes1 is a downstream target gene in the Notch signaling pathway, which is related to cell proliferation and self-renewal [24]. To determine if ERK1/2 signaling pathways and Hes1 were involved in the proliferation and maintaining of stem/progenitor cells, phosphorylation of ERK1/2 and Hes1 was evaluated by western blot analysis following RSV treatment. Meanwhile, activation of Sirt1 by RSV was also detected with western blot analysis. The multipotent C17.2 NPC line served as an in vitro model to explore the manners of EtOH or RSV on NPC proliferation.

2. Materials and methods

2.1. Animals

Male and female C57/BL6 mice were provided by the Third Military Medical University and were housed in a temperature-controlled room with a standard 12-h light/12-h dark cycle and ad libitum access to food and water. All experimental procedures were approved by Third Military Medical University and were performed according to the guidelines of laboratory animal care and use.

2.2. Drug treatment

The day of birth was designated as postnatal day 0 (P0). On P6, pups were randomly divided into the following four groups: (1) pretreatment with 100% dimethyl sulfoxide (DMSO) followed by normal saline (0.9% NaCl) (DMSO + NS), (2) pretreatment with RSV followed by normal saline (0.9% NaCl) (RSV + NS), (3) pretreatment with DMSO followed by alcohol (DMSO + EtOH), or (4) pretreatment with RSV followed by alcohol (RSV + EtOH). RSV (dissolved in 100% DMSO) was intraperitoneally (i.p.) injected (20 mg/kg) at P6 as previously described [21]. The control groups received an equivalent dose of vehicle DMSO. On P7, animals pretreated with either DMSO or RSV were intraperitoneally (i.p.) injected with a total of 5 g/kg (2.5 g/kg at time of 0 h and 2 h, respectively) EtOH (20% EtOH in sterile normal saline) according to our previously described methods [25]. The controls were injected with an equivalent volume of sterile saline (i.p.). To avoid the litter-effect, the animals in each treatment group were randomly chosen from multiple litters, one pup per litter was selected for each of the group. In this study, we used a minimum number of mice that were required to draw the conclusions and tried to minimize their suffering as much as possible.

BrdU (Sigma-Aldrich) was dissolved in 0.9% saline. To assess cell proliferation in the DG, the pups received one injection of BrdU at a dose of 50 mg/kg per injection (i.p.) on P8 (24 h after the first EtOH injection) and were sacrificed 2 h after the BrdU administration. To analyze neurogenesis in the DG, the pups were administered BrdU (50 mg/kg i.p. four times over 24 h) on P8 and were then sacrificed on P14.

2.3. Immunohistochemistry and immunofluorescence

The brain was dissected and fixed in 4% paraformaldehyde (PFA) for 24 h at 4 °C. For paraffin sections, tissues were processed for paraffin embedding, and coronal sections (5 μm thick) were collected. The remaining brains were post-fixed in a 30% sucrose solution with 4% PFA at 4 °C, and coronal cryosections (15 μm thick at P8, 20 μm thick at P14) were collected. Paraffin sections were used for hematoxylin–eosin (HE) staining to examine the cytoarchitecture of the hippocampus. Immunohistochemistry was performed according to Yang et al. [25]. In brief, sections were exposed to the following primary antibodies in 1% BSA (12 h, 4 °C): anti-Nestin (1:400) (BD Biosciences), anti-BLBP (1:400), anti-Sox2 (1:500) and anti-glial fibrillary acidic protein (GFAP) (1: 100) (Chemicon, Temecula, CA, USA), and 1% BSA replaced primary antibodies in negative controls. For BrdU staining, all the sections were pretreated with 2 N HCl for 1 h at 37 °C to denature the DNA followed by 0.1 M borax (pH 8.5) treatment for 10 min to neutralize before the regular immunostaining procedure. After washing the samples in PBS for BrdU staining, the sections were incubated with biotin-conjugated secondary antibody and were visualized under bright-field microscopy with a diaminobenzidine substrate kit (Vector Laboratories, Burlingame, CA, USA). For immunofluorescence, the sections were then incubated with Cy3- or 488-conjugated (both at 1:400, 3 h; Jackson ImmunoResearch, West Grove, PA, USA) secondary antibodies and mounted in Vectashield (Vector). Nuclei were subsequently stained with 4′,6-diamidino-2-phenylindole (DAPI, Beyotime, China). The stained cells were viewed and photographed under a Zeiss (Oberkochen, Germany) Axivert microscope equipped with a Zeiss AxioCam digital color camera connected to the Zeiss AxioVision 3.0 system.

2.4. Western blotting

Hippocampi were isolated and homogenized in ice-cold RIPA lysis buffer (Beyotime, Shanghai, China). After centrifugation of lysates (15,000 *g*, 5 min at 4 °C), the protein concentration was determined via the Bicinchoninic Acid Kit (Beyotime Institute of Biotechnology, Shanghai, China). Protein samples (40 μg per lane) were separated on a 12% SDS-polyacrylamide gel and then transferred onto polyvinylidene fluoride (PVDF) membranes for immunoblotting. The membranes were blocked with Tris-buffered saline (TBS) containing 0.1% Tween 20 (TBST) and 5% fat-free milk for 1 h at RT. The membranes were then incubated (overnight at 4 °C) with rabbit antibodies against Hes1 (1:1000, Chemicon), p-ERK1/2 or total-ERK1/2 (1:1000, Cell Signaling), Sirt1 (1:1000, Chemicon) and β-actin (1:2000, Cell CWBIO, Beijing, China), followed by 1 h of RT incubation with a peroxidase-conjugated goat anti-rabbit immunoglobulin G (IgG, 1:2000; Santa Cruz Biotechnology). All western blotting data were representative of at least three independent experiments. Specific protein bands on the membranes were visualized by the enhanced chemiluminescence method (Amersham, Piscataway, NJ, USA) according to the manufacturer's instructions. The relative intensities of Hes1, Sirt1 and p-ERK were normalized to the internal

reference protein β-actin or total ERK and then normalized to the control group.

2.5. Golgi staining

The brains were quickly removed and prepared for Golgi staining using the Rapid Golgi Stain Kit (FD NeuroTechnologies, Ellicott City, MD, USA) according to our previously described methods [25]. In brief, the brains were incubated in impregnation solution for 2 weeks at room temperature under dark conditions. After staining, brain coronal sections (80 μm thick) were mounted on slides, dehydrated with xylene, and then mounted with a coverslip using Permount Mounting Media (Fisher Scientific, Pittsburgh, PA). Granule neurons in an identical area of the hippocampal SGZ were selected from each group, and one or two dendritic segments of equal length from each neuron were chosen for quantification. The density and morphology of dendritic spines were manually quantified according to the criteria described by Chakraborti et al. [26].

2.6. Quantification

2.6.1. Determination of dentate gyrus cell number

Paraffin sections from animals were cut serially (5 μm thickness) through the rostrocaudal extent of the hippocampus. The number of cells in the hilus (between the two blades of the granule cell layer) and the granule cell layer (GCL; which included SGZ) was counted on nine matched sections of the caudal, medial as well as the rostral hippocampi per animal and the average value of a section per animal was determined. Six animals per group were used for analysis.

2.6.2. Determination of RGCs in the DG labeled by SOX2/GFAP and BLBP/Nestin at P8

Cryostat sections (15 μm thickness) were double-immunofluorescently stained with SOX2/GFAP and BLBP/Nestin respectively. The somata of radial glia have a triangular shape and the processes are marked by GFAP, BLBP or Nestin and usually project toward the molecular layer. Double stained sections in the GCL

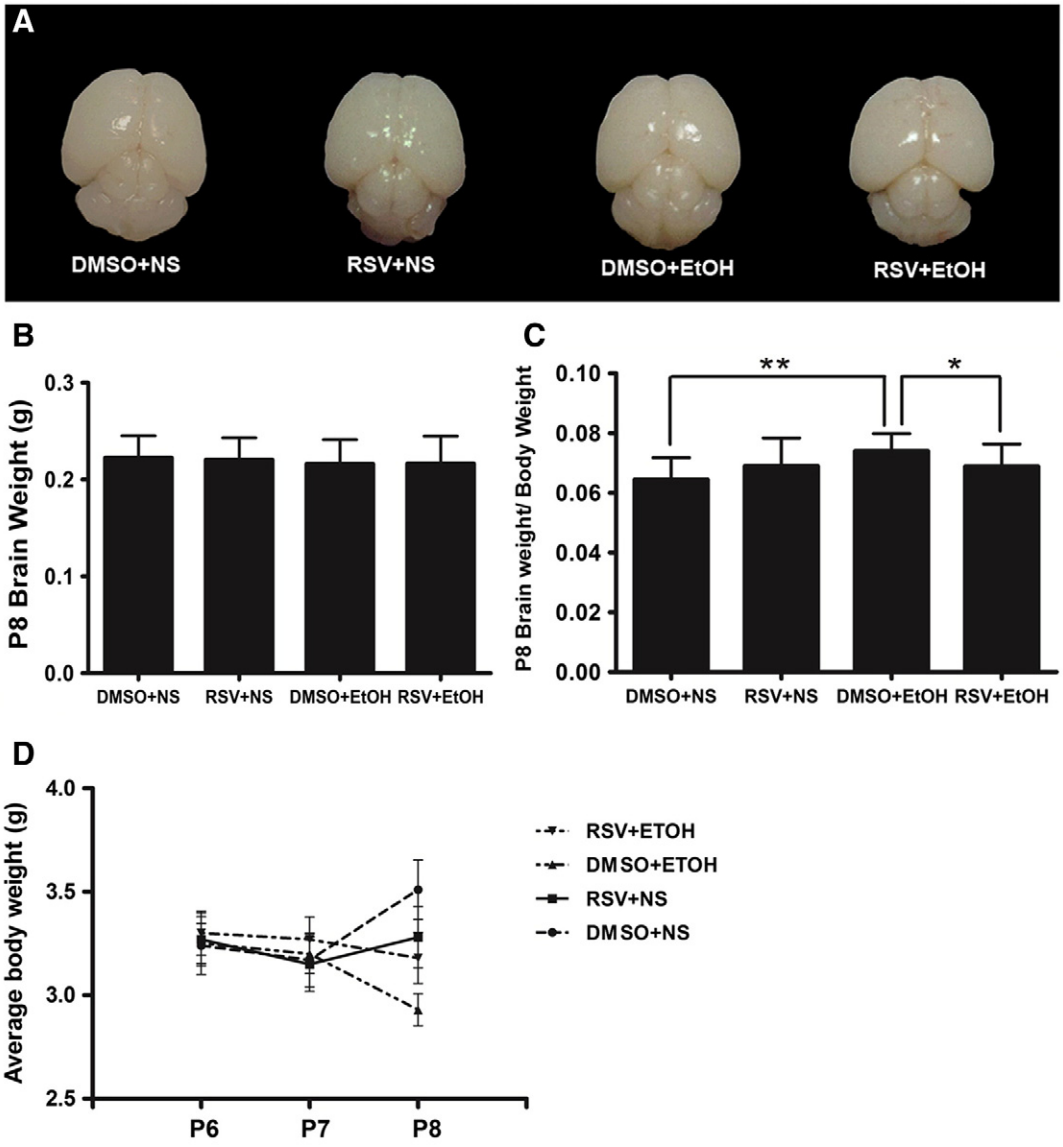

Fig. 1. Effects of EtOH and RSV on average body weight and brain weight/body weight ratio. (A) No alterations were found in the gross morphology of the brains from each of the four groups. (B) The effects of EtOH and RSV on the average brain weight of mouse pups. (C) The effects of EtOH and RSV on the brain weight/body weight ratio. (D) The effects of EtOH and RSV on the average body weight of mouse pups. Data are presented as mean ± SEM ($n = 20$). *$p < 0.05$; **$p < 0.01$.

(plus SGZ) of nine matched sections of the caudal, medial as well as the rostral hippocampi per animal were counted and the average value of a section per animal was determined. Five animals per group were used for analysis.

2.6.3. Stereological quantification of BrdU positive cells in the DG at P8, BrdU-positive DCX/BrdU-positive cells and GFAP/BLBP-positive cells in the DG at P14

Every 10th section (40 μm thickness), for animals sacrificed at P8 throughout the hippocampus was used to determine the total number of BrdU in the entire DG (GCL plus SGZ and hilus) under light microscopy in each animal. The total sum of the BrdU positive cells traced was multiplied by BrdU positive cells per section and series number to give the total number of BrdU positive cells in the DG. Six animals per group were used for analysis.

Serial 20 μm sections through the rostrocaudal extent of the DG were selected at ten-section intervals for immunofluorescent staining with the BrdU/DCX and GFAP/BLBP and counterstaining with DAPI to mark nuclei in the DG at P14. The total sum of the BrdU or BrdU/DCX positive cells traced were multiplied by positive cells in the GCL (plus SGZ) per section and series number to give the total number of BrdU or BrdU/DCX positive cells in the DG. The total sum of the GFAP/BLBP positive cells traced were multiplied by positive cells in the SGZ (at the junction between the granule cell layer and the hilus) per section and series number to give the total number of GFAP/BLBP positive cells in the SGZ. Five animals per group were used for analysis.

2.7. C17.2 NPC culture and drug treatment

According to our previous methods [27,28], the C17.2 cells were cultured in standard DMEM/F12 (Invitrogen) containing 10% fetal calf serum (FCS, Gibco, USA), 5% horse serum and 2 mM glutamine at 37 °C in the presence of 5% CO_2. To evaluate the effect of pretreatment of RSV on NPCs, 5 μM RSV (dissolved in DMSO) and equivalent DMSO were added into the culture medium of C17.2. For analysis of cell proliferation and cell cycle, C17.2 was plated into 6-well plate and coverslips within 24-well plate (cell density, 4×10^4/ml/coverslip) respectively. After 12 h pretreatment, RSV and DMSO were washed out and added EtOH (700 mg/dl) or 0.01 M PBS respectively. After 12 h or 36 h exposure to EtOH, C17.2 cells were collected for assay.

2.8. Cell proliferation and apoptosis assay of C17.2

The cell proliferation assay of C17.2 was performed according to our previous methods [27,29]. In brief, C17.2 cells were fixed with 4% PFA for 15 min at room temperature. After using 0.1% Triton X-100 to permeabilize for 10 min, the cells were blocked with 3% BSA (Sigma-Aldrich) and 10% normal goat serum (Boster, China) for 1 h at room temperature. The cells were then incubated with rabbit anti-Ki67 antibody (1:300, Abcam, UK) overnight at 4 °C. After washing three times with PBS, the cells were incubated with secondary antibodies (Alexa Fluor® 568 goat anti-rabbit IgG, 1:500; Life Technologies, USA) for 1 h at 37 °C. Nuclei were stained with DAPI (Beyotime, China).

The apoptosis of C17.2 was analyzed with In Situ Cell Death Detection Kit (Roche, Indianapolis, IN) according to the manufacturer's instructions. In brief, cells were fixed with 4% PFA, permeabilized with 0.1% Triton X-100 and incubated with a mixture of enzyme solution (TdT) and Label Solution (fluorescein-dUTP; 1:9) for 1 h at 37 °C, after washing three times with PBS, the nuclei of the cells were stained with DAPI (Beyotime, China). After immunostaining, the cells were observed and analyzed using a fluorescence microscopy system

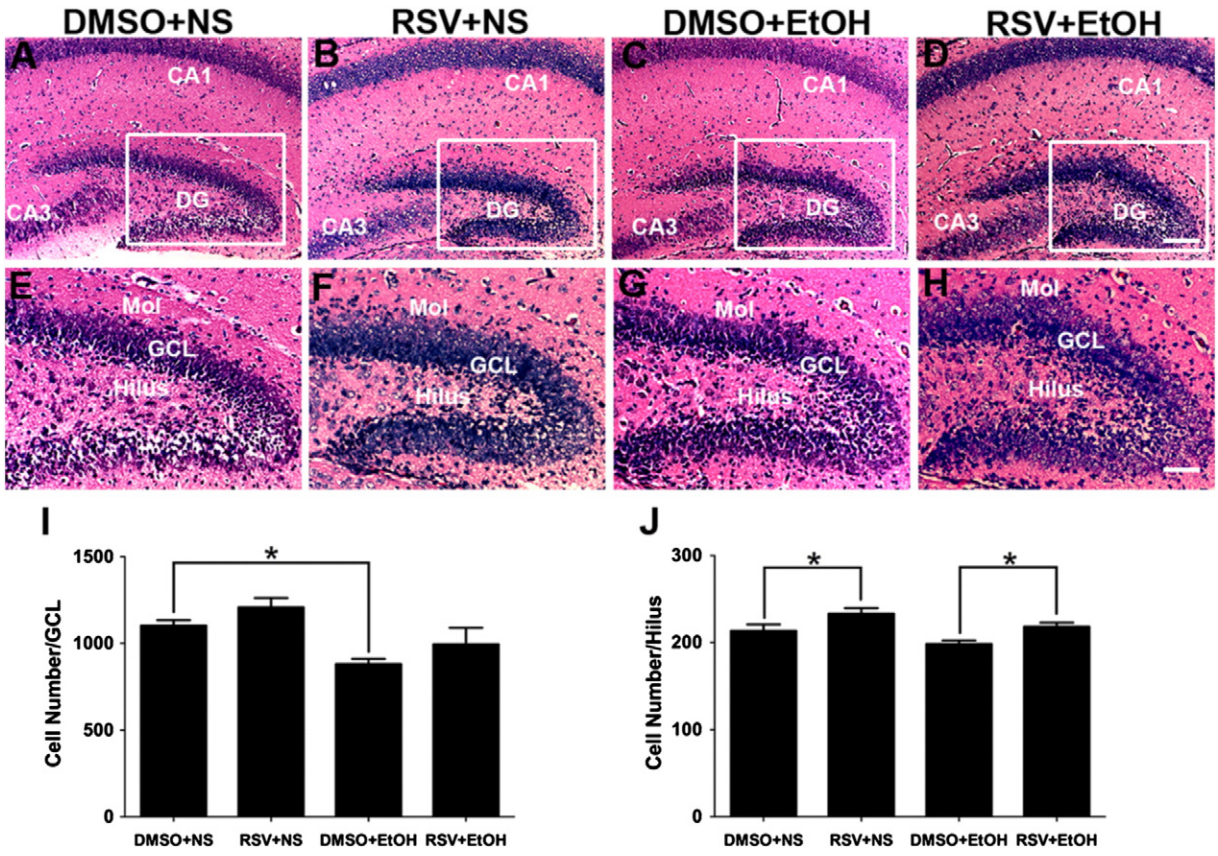

Fig. 2. Pretreatment with RSV rescues the EtOH-mediated decline in granule cells in the DG at P8. The DG structure of the hippocampus as shown by HE staining for the groups: (A) DMSO + NS; (B) RSV + NS; (C) DMSO + EtOH; and (D) RSV + EtOH. (E–H) Images are higher-power views of the boxed areas in A–D. (I) Cell number analysis in the GCL. (J) Cell number analysis in the hilus. Data are presented as mean ± SEM ($n = 6$). *$p < 0.05$. Scale bar in D = 100 μm and applies to A–D, in H = 50 μm and applies to E–H.

(Leica, Germany). At least 10 fields were counted for each slide. The ratio of Ki67-positive or Terminal Deoxy Nucleotidyl Transferase-Mediated Nick End Labeling (TUNEL) stained cells was determined by calculating positive cells to the total number of cells in each field. Measurements were all repeated at least three times.

2.9. FACS analysis of the cell cycle of C17.2 cells

The C17.2 cells were dissociated by trypsin-EDTA (Gibco). After centrifugation and washing with PBS twice, the cells were harvested according to our previous protocol [29]. The cells were fixed in 70% EtOH overnight at 4 °C, then stained with the Cycletest™ Plus DNA Reagent Kit (BD). The results were detected by a FACSCalibur flow cytometer and analyzed by the ModFit 2.0 software (BD). For each sample, at least 20,000 cells were analyzed and all the analyses were performed in three independent experiments.

2.10. Statistical analysis

Statistical analysis was performed with two-way ANOVA followed by Bonferroni post-hoc test and one-way ANOVA followed by LSD post-hoc analysis for multiple comparisons using SPSS 13.0 software (SPSS Inc., Chicago, IL, USA). Data are presented as mean ± SEM. A p-value of less than 0.05 was considered statistically significant.

3. Results

3.1. Effects of EtOH and RSV on average body weight and brain weight/body weight ratio

No obvious gross morphological differences were observed in the brain after treatment with EtOH or RSV (Fig. 1A). There was no effect of time [$F(2,76) = 1.378$; $p = 0.244$] and treatment group [$F(3,76) = 0.464$; $p = 0.709$] on the body weight, while significant interaction was detected between factors [$F(6,76) = 6.574$; $p < 0.01$]. The average body weight of mice at P8 in the DMSO + EtOH group was significantly lower ($p < 0.01$) compared with those in the DMSO + NS group (Fig. 1D). No significant difference was found in the mean brain weight between the four groups (Fig. 1B). However, the brain weight/body weight ratio was significantly higher ($p < 0.01$) in the EtOH-treated group (Fig. 1C). Compared with EtOH treatment, this ratio was lower in the RSV-treated EtOH-exposed pups ($p < 0.05$) (Fig. 1C).

3.2. Pretreatment with RSV rescues the EtOH-mediated decline of granule cells in the DG

To examine the structural integrity of the hippocampus, coronal sections of the hippocampus of each of the four groups were compared. Analysis of these sections indicated that the hippocampal structure was similar in the pups at P8 as visualized with HE staining, and no

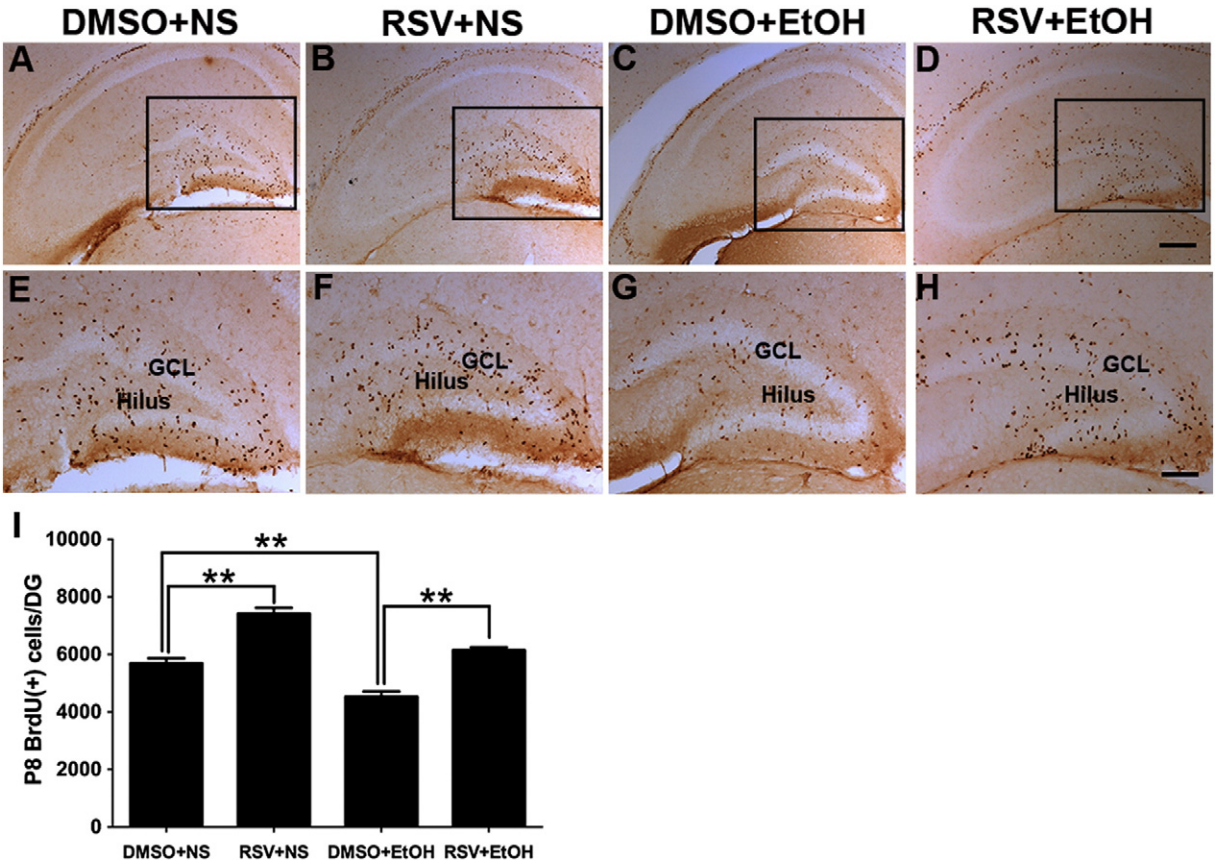

Fig. 3. Pretreatment with RSV antagonized the EtOH-mediated inhibition of cell proliferation in the DG at P8. (A–H) Representative images of BrdU-immunolabeled coronal sections of the DG of the groups treated with DMSO + NS (A and E), RSV + NS (B and F), DMSO + EtOH (C and G) and RSV + EtOH (D and H). (E–H) Images are higher-power views of the boxed areas in (A–D). (I) Quantitative analysis of the number of BrdU-labeled cells in the hippocampal DG. Data are presented as mean ± SEM ($n = 6$). $^{**}p < 0.01$. Scale bar in D = 200 μm and applies to A–D, in H = 100 μm and applies to E–H.

differences in the morphology or area size were observed in the DG between the groups (Fig. 2). The GCL of the DG in the DMSO + EtOH group (Fig. 2C, G, I) appeared less dense than that in the DMSO + NS group ($p < 0.05$) (Fig. 2A, E, I), and this reduction in density could be partially rescued by RSV pretreatment (Fig. 2D, H, I). Furthermore, cellular density in the hilus of the DMSO + NS group (Fig. 2A, E, I) and DMSO + EtOH group (Fig. 2C, G, I) could be increased by RSV treatment (Fig. 2B, F, D, H, J).

3.3. Pretreatment with RSV antagonized the EtOH-mediated inhibition of cell proliferation in the DG

Twenty-four hours after BrdU administration, intense BrdU labeling of proliferating cells was observed in the DG of 8-day-old mice. The most intense BrdU-labeled cells were found in the GCL and hilus, and scattered cells were also observed in the molecular layer (Fig. 3). Newly born cells were irregularly shaped and often appeared in clusters. RSV administration (Fig. 3B, F) increased the number of BrdU-positive cells in the DG (DMSO + NS, 5688 ± 178 cells; RSV + NS, 7418 ± 203 cells, $p < 0.01$, Fig. 3I). In contrast, BrdU-labeled cells in the DG were significantly decreased ($p < 0.01$, Fig. 3I) in the DMSO + EtOH group (Fig. 3C, G). Compared with the DMSO + EtOH group (Fig. 3C, G), mice pretreated with RSV (Fig. 3D, H) significantly restored the reduction of BrdU-labeled cells in the DG ($p < 0.01$) (Fig. 3G, H, I).

3.4. Pretreatment with RSV reverses the EtOH-mediated exhaustion of the NPC pool in the DG of the 8-day-old mice

A decrease in cellular proliferation in the hippocampus may be due to a decline in the number of stem/progenitor cells available in the GCL. To test this hypothesis, we examined the expression of SOX2, a transcription factor expressed in both stem cells and putative precursor cells required for stem cell maintenance [30]. EtOH administration decreased SOX2-positive neural stem/early progenitor cells by 15% (DMSO + EtOH, 231 ± 5 cells; DMSO + NS, 270 ± 6 cells; $p < 0.01$, Fig. 4I). Compared with the DMSO + EtOH group, mice pretreated with RSV significantly restored the number of $SOX2^+$ neural stem/early progenitor cells in the GCL. Postnatally, RGCs are transformed into NPCs in the DG as GFAP- and Nestin-positive cells and are the source of continuous neurogenesis throughout life. To further explore the defects in the NPC pool in mice treated with EtOH, we determined the number of NPCs and their progeny using various lineage markers. Indeed, EtOH exposure decreased the pool of NPCs in the DG significantly at P8 compared with the DMSO + NS group, as measured by their radial glial morphology with the expression of both GFAP and SOX2 (149 ± 3 versus 178 ± 4 per section, $n = 5$ mice, $p < 0.01$, Fig. 4J) or BLBP and Nestin (91 ± 5 versus 106 ± 4 per section, $n = 5$ mice, $p < 0.01$, Fig. 5I). Moreover, the decrease in the NPC pool induced by EtOH in the DG, as measured by $GFAP^+/SOX2^+$ (Fig. 4A–H) and $BLBP^+/Nestin^+$ (Fig. 5A–H) cells with a radial glial morphology, was also rescued by RSV pretreatment to values similar

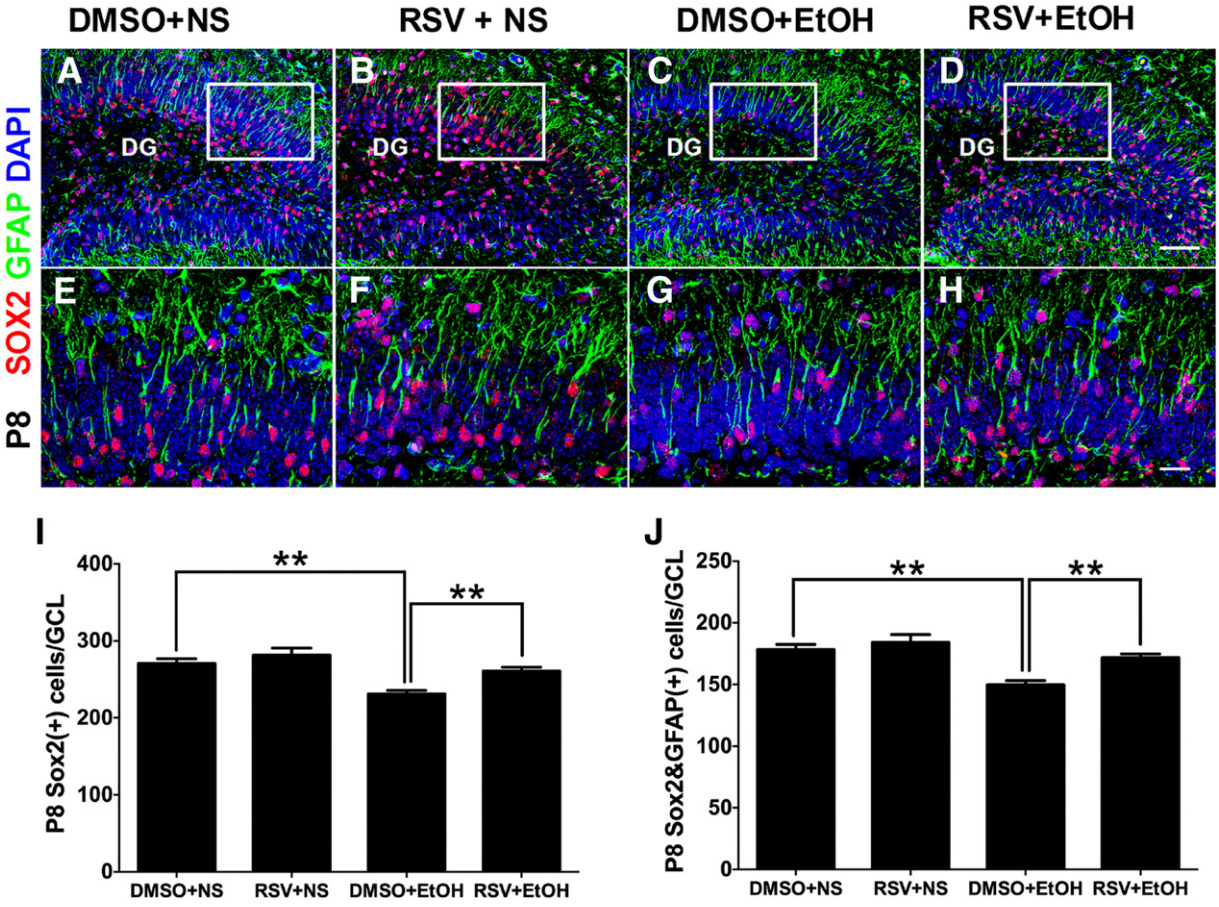

Fig. 4. Pretreatment with RSV rescues the EtOH-mediated decline in RGCs labeled with GFAP and SOX2 in the DG. (A–H) Representative images of SOX2 and GFAP double-positive RGCs in the DG of the groups treated with DMSO + NS (A and E), RSV + NS (B and F), DMSO + EtOH (C and G) and RSV + EtOH (D and H). (E–H) Images are higher-power views of the boxed areas in A-D. (I) Quantitative analysis of the number of SOX2-positive cells in the GCL. (J) Quantitative analysis of the number of SOX2- and GFAP-positive cells in the GCL. Data are presented as mean ± SEM ($n = 5$). $^{**}p < 0.01$. Scale bar in D = 50 μm and applies to A–D, in H = 25 μm and applies to E–H.

to those in mice from the DMSO + NS group (Figs. 4, 5). Together, these results indicate that RSV can rescue the defects in the NPC pool caused by EtOH exposure.

3.5. RSV restores the EtOH-mediated decline in hippocampal neurogenesis

To assess the impact of EtOH and RSV on early postnatal hippocampal neurogenesis, we administered BrdU at P8 and analyzed the number of $BrdU^+$ nuclei as well as cells positive for both BrdU and DCX (marker for migrating neuroblasts, or newly formed neurons) in the DG at P14 (Fig. 6A–D). EtOH exposure decreased both the number of $BrdU^+$ cells and $BrdU^+/DCX^+$ cells in the GCL by around 27% ($p < 0.01$, Fig. 6E, F), compared with the DMSO + NS group. In contrast to the DMSO + EtOH group, RSV pretreatment increased the number of $BrdU^+$ cells and $BrdU^+/DCX^+$ cells by 28% ($p < 0.01$, Fig. 6E) and 31% ($p < 0.01$, Fig. 6F) respectively. These findings suggest that EtOH, when administered to infant mice at P7, suppressed neurogenesis within the hippocampal DG, and this suppression can be rescued by RSV pretreatment. Moreover, EtOH exposure significantly decreased the number of NPCs in the DG at P14 by 30% compared with the DMSO + NS group as measured by their radial glial morphology and expression of both GFAP and BLBP (Fig. 7A–H). Compared with the DMSO + EtOH group, mice pretreated with RSV significantly restored the reduced $GFAP^+/BLBP^+$ labeled cells in the DG ($p < 0.01$, Fig. 7I). Moreover, RSV alone increased RGCs that were double labeled with GFAP and BLBP by 14%.

3.6. Pretreatment with RSV rescues EtOH-mediated impairments in the density of total dendrites and mushroom spines

We next investigated whether EtOH exposure leads to spine degeneration. We imaged the dendritic spines in the granular neurons of each of the four groups on P14 and determined their density and characteristics (Fig. 8). The results showed that the number of the dendritic spines per 10 μm was significantly reduced in the spared granular neurons of EtOH exposed mice (DMSO + EtOH, 9.8 ± 0.9; DMSO + NS, 12.3 ± 0.3; $p < 0.05$, Fig. 8E). In contrast to the DMSO + EtOH group, RSV pretreatment increased the density of dendritic spines to values similar to those in mice from the DMSO + NS group. This result indicates that a reduction in the number of dendritic spines in the spared neurons following EtOH exposure can be restored by RSV.

The morphological changes in spines are related to the strength of their synaptic contacts. In this regard, the dendritic spine protrusions have been conventionally classified as stubby, thin or mushroom-shaped. In contrast to the DMSO + NS group, we found that EtOH exposure caused a dramatic decrease in the proportion of mushroom-shaped spines (DMSO + EtOH, 27.3 ± 3.9%; DMSO + NS, 45.7 ± 3.1%; $p < 0.01$, Fig. 8G) and a concomitant higher proportion of stubby spines (DMSO + EtOH, 53.9 ± 4.0%; DMSO + NS, 33.3 ± 2.0%; $p < 0.01$, Fig. 8H), but no change in the proportion of thin spines was found (Fig. 8I). However, RSV pretreatment decreased the proportion of stubby spines and increased the proportion of mushroom-shaped spines.

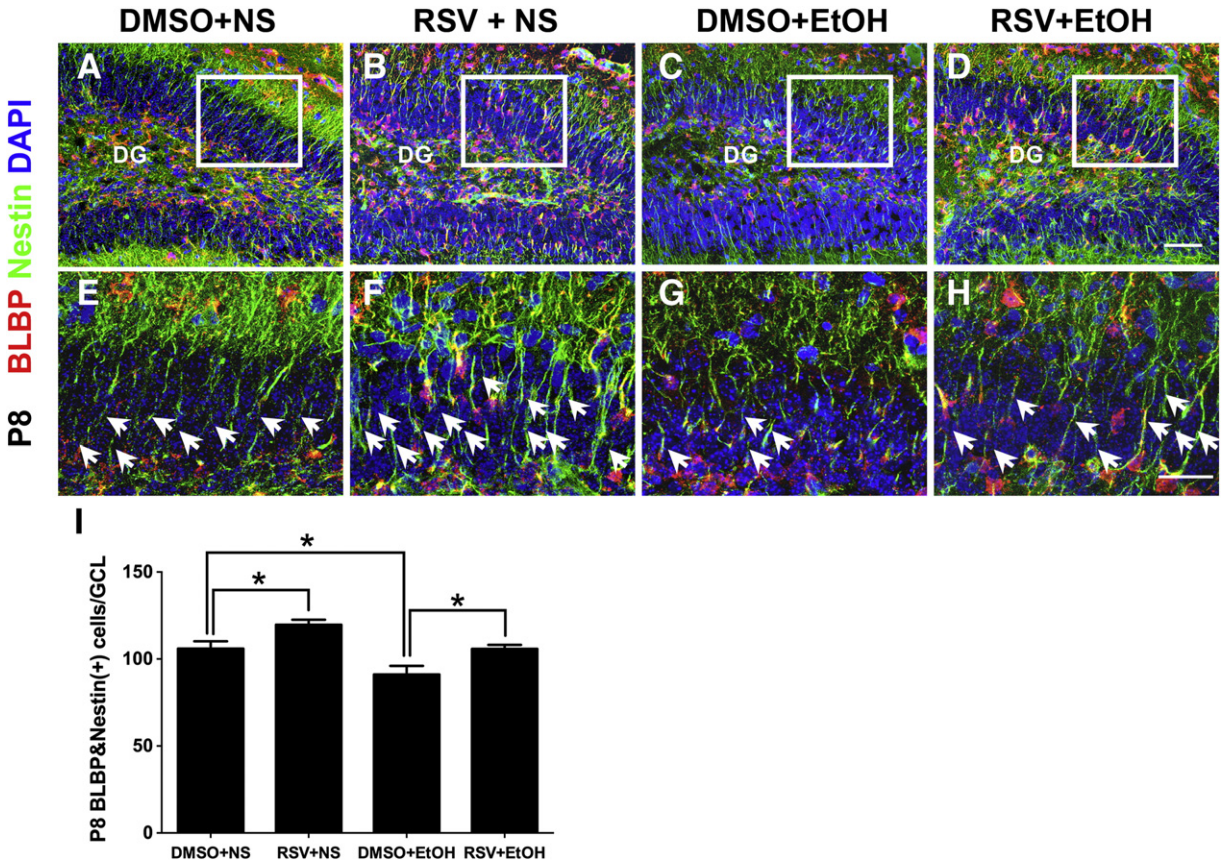

Fig. 5. Pretreatment with RSV rescues the EtOH-mediated decline in the RGCs labeled by BLBP and Nestin in the DG. (A–H) Representative images of BLBP- and Nestin-double-positive RGCs in the DG of groups treated with DMSO + NS (A and E), RSV + NS (B and F), DMSO + EtOH (C and G) and RSV + EtOH (D and H). (E–H) Images are higher-power views of the boxed areas in A–D. Arrowheads indicate the $BLBP^+/Nestin^+$ double staining cells. (I) Quantitative analysis of the number of $BLBP^+/Nestin^+$ in the GCL. Data are presented as mean ± SEM ($n = 5$). *$p < 0.05$. Scale bar in D = 50 μm and applies to A–D, in H = 25 μm and applies to E–H.

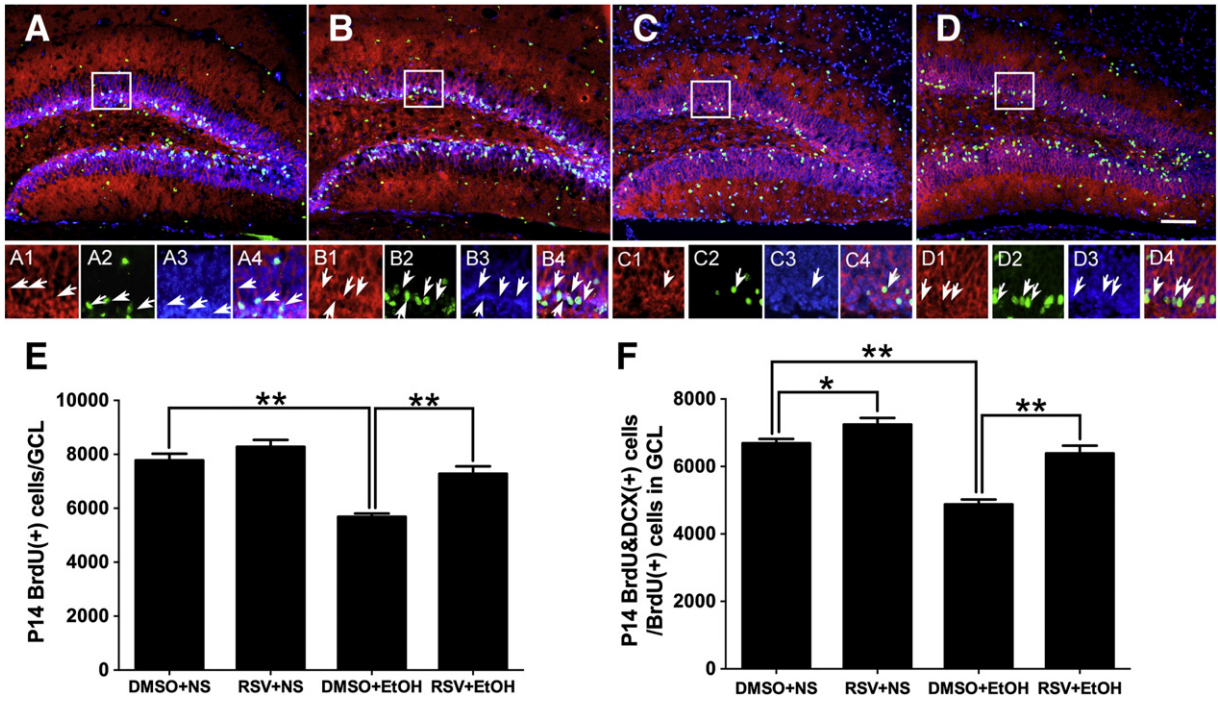

Fig. 6. RSV restores the EtOH-mediated decline in hippocampal neurogenesis. Immunolabeling for BrdU (green), DCX (red), and DAPI (blue) in the mouse DG of groups treated with DMSO + NS (A), RSV + NS (B), DMSO + EtOH (C) and RSV + EtOH (D). (E) Quantitative analysis of the number of BrdU-positive cells in the GCL. (F) Quantitative analysis of the number of DCX- and BrdU-double stained cells in the GCL. Data are presented as mean ± SEM ($n = 5$). $^{*}p < 0.05$; $^{**}p < 0.01$. Scale bar in D = 100 μm and applies to A–D.

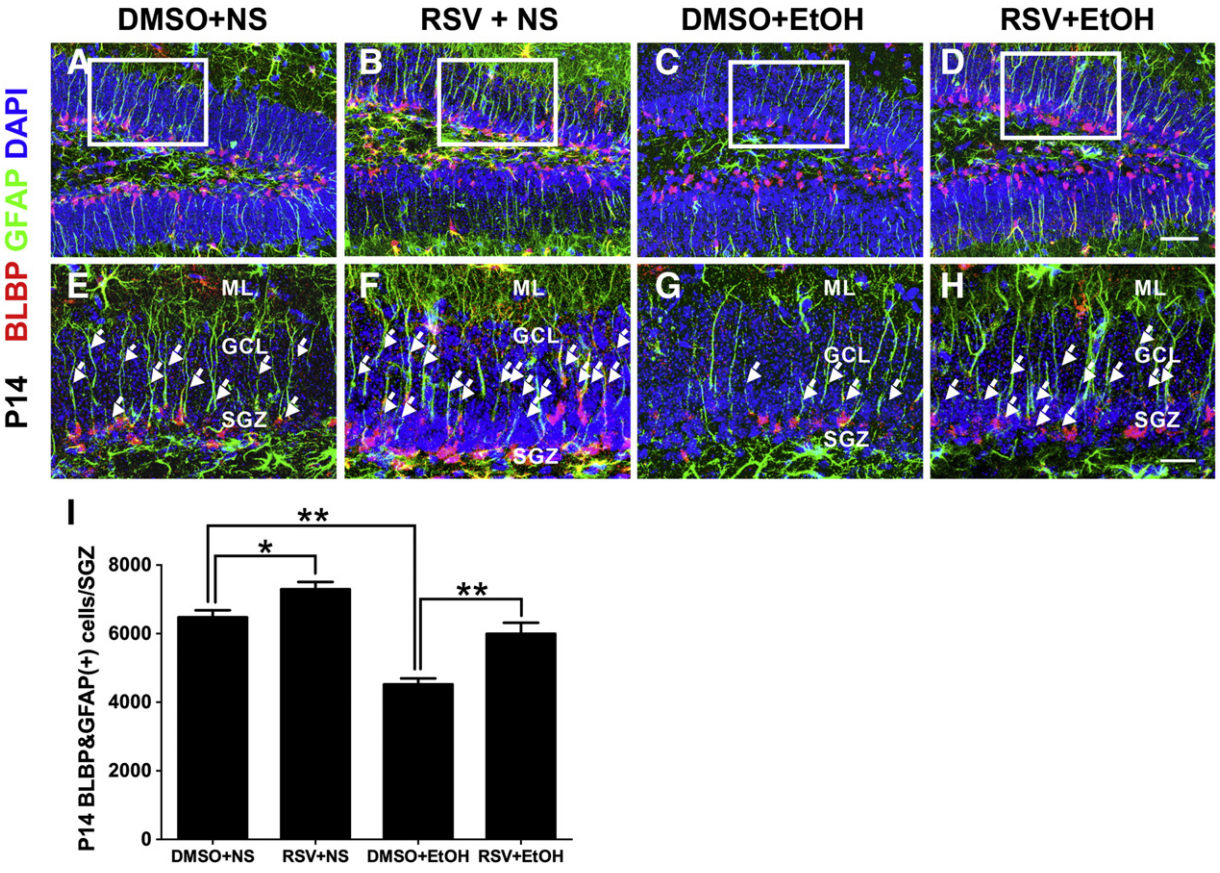

Fig. 7. Pretreatment with RSV rescues the EtOH-mediated decline in BLBP- and GFAP-double stained cells in the SGZ of P14 mice. (A–H) Representative images of BLBP- and GFAP-double positive RGCs in the DG of groups treated with DMSO + NS (A and E), RSV + NS (B and F), DMSO + EtOH (C and G) and RSV + EtOH (D and H). (E–H) Images are higher-power views of the boxed areas in A–D. Arrowheads indicate the $BLBP^{+}/GFAP^{+}$ double staining cells. (I) Quantitative analysis of the number of $BLBP^{+}/GFAP^{+}$ double stained cells in the SGZ. Data are presented as mean ± SEM ($n = 5$). $^{*}p < 0.05$; $^{**}p < 0.01$. Scale bar in D = 50 μm and applies to A–D, in H = 25 μm and applies to E–H.

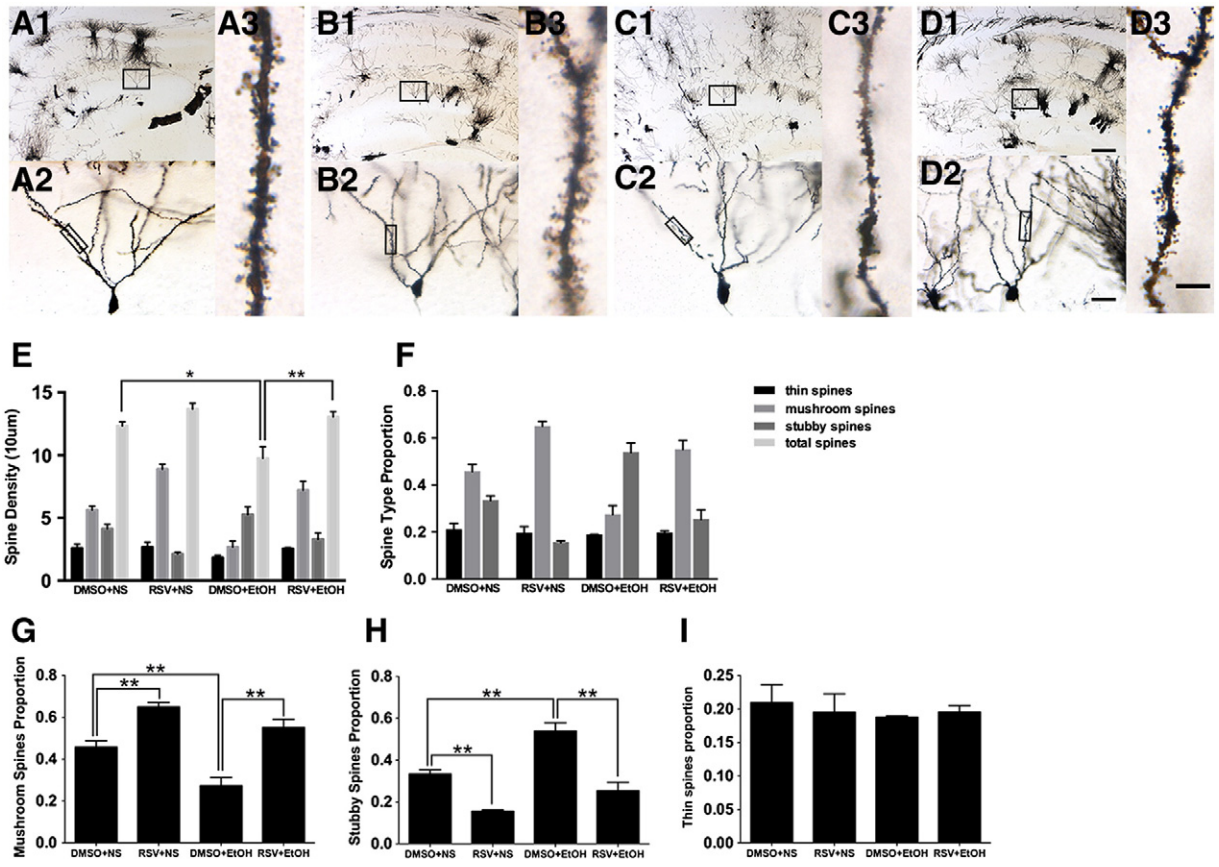

Fig. 8. Pretreatment with RSV rescues EtOH-mediated impairments in the dendritic spines of DG granule neurons. Representative images of Golgi-impregnated dentate gyri (A1–D1), granule cells (A2–D2), and dendritic spines (A3–D3) in the hippocampus of P14 mice from groups treated with DMSO + NS (A1, A2 and A3), RSV + NS (B1, B2 and B3), DMSO + EtOH (C1, C2 and C3) and RSV + EtOH (D1, D2 and D3). (E) Quantitative analysis of dendritic density on granule cells. (F) Overall changes in the proportions of spine morphological subtypes in the DG granule neurons. Quantitative analysis of the proportions of mushroom spines (G), stubby spines (H), and thin spines (I). Data are presented as mean ± SEM ($n = 3$); $^{*}p < 0.05$; $^{**}p < 0.01$. Scale bar in D1 = 100 μm and applies to A1–D1, in D2 = 20 μm and applies to A2–D2, in D3 = 5 μm and applies to A3–D3.

3.7. RSV rescues the EtOH-mediated decline in the protein levels of pERK1/2 Hes1 and Sirt1 in the hippocampus

To investigate the molecular mechanisms mediating the proliferation of NPCs in EtOH- or RSV-treated mice, we performed western blotting to assess if the expression levels of phospho-ERK1/2 (pERK1/2) in the hippocampus at P8 were affected by EtOH or RSV treatment. We found that RSV alone increased ERK1/2 phosphorylation level in the hippocampus by 65% compared with the DMSO + NS group ($p < 0.05$). In agreement with published studies [31,32], the hippocampal ERK1/2 phosphorylation level of the mice in the DMSO + EtOH group was 14% lower (but not significantly) compared with those in mice from the

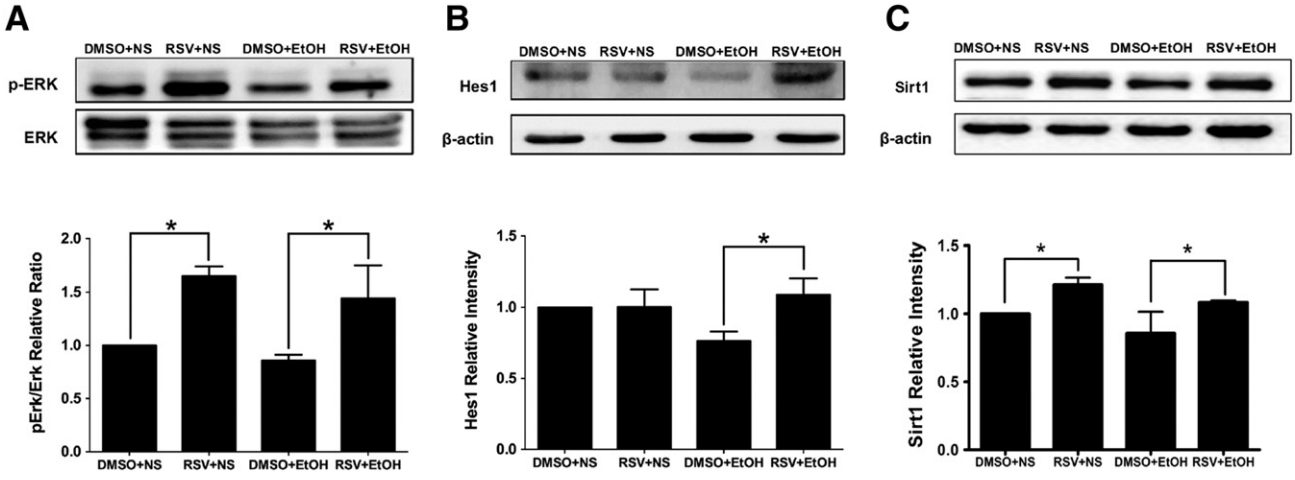

Fig. 9. RSV rescues the EtOH-mediated decline in the protein levels of pERK1/2, Hes1 and Sirt1 in the hippocampus at P8. (A) Top: representative immunoblots of phosphorylated ERK and total ERK. Bottom: graph representing the densitometric analysis of pERK/ERK. (B) Top: representative immunoblots of Hes1. Bottom: graph representing the densitometric analysis of Hes1. (C) Top: representative immunoblots of Sirt1. Bottom: graph representing the densitometric analysis of Sirt1. Data are presented as mean ± SEM ($n = 3$); $^{*}p < 0.05$.

DMSO + NS group ($p < 0.05$). The decrease of the pERK1/2 protein by EtOH was reversed by RSV pretreatment (Fig. 9A). Hes1 has been indicated to be essential for maintenance of RGCs [33]. Therefore, we further detected Hes1 levels in the hippocampi of mice from each of the four groups. We found that EtOH exposure decreased Hes1 levels by 24% (but not significantly) lower compared with those in mice from the DMSO + NS group. The decrease in Hes1 protein levels by EtOH was almost completely reversed by RSV treatment ($p < 0.05$) (Fig. 9B). We also noticed that RSV pretreatment increased the Sirt1 level in the hippocampus after the EtOH exposure (Fig. 9C), suggesting that Sirt1 activation by RSV might be involved in the reversed inhibition of pERK and Hes1 induced by EtOH exposure.

3.8. RSV pretreatment blocked the EtOH exposure induced apoptosis and proliferation declines of NPCs

The ratio of Ki67-positive cells was used to analyze the cell proliferation. It showed a significant decrease in the ratio of Ki67-positive cells after EtOH exposure 12 h compared with DMSO treatment (Fig. 10A, C, Q). RSV treatment alone for 12 h significantly increased the ratio of Ki67-positive cells compared with DMSO + PBS group (Fig. 10A–B, E–F). Meanwhile, pretreatment with RSV antagonized the effect of EtOH exposure (both for 12 h and 36 h) on NPC proliferation, as the ratio of Ki67-positive cells was significantly increased compared with EtOH group (Fig. 10C–D, G–H, Q). The apoptosis analysis was carried out via TUNEL staining. After exposed to EtOH for 12 h and 36 h, the ratio of TUNEL-positive cells was significantly increased compared with the DMSO + PBS group (Fig. 10I, K, M, O, R), which could be reversed by pretreatment with RSV for 12 h (Fig. 10I–P).

3.9. RSV pretreatment antagonized the EtOH exposure induced mitotic cell cycle arrest

The cell cycle analysis also demonstrated that EtOH exposure for 12 h and 36 h inhibited the cell mitosis significantly compared with the DMSO + PBS group (Fig. 11A, C, E, G, I, J). However, RSV treatment alone promotes the mitosis of NPCs significantly compared with DMSO + PBS group (Fig. 11A–B, E–F, I–J). Compared with EtOH exposure group, pretreatment of RSV significantly blocked the mitotic cell cycle arrest of NPCs (Fig. 11C–D, G–H, I, J).

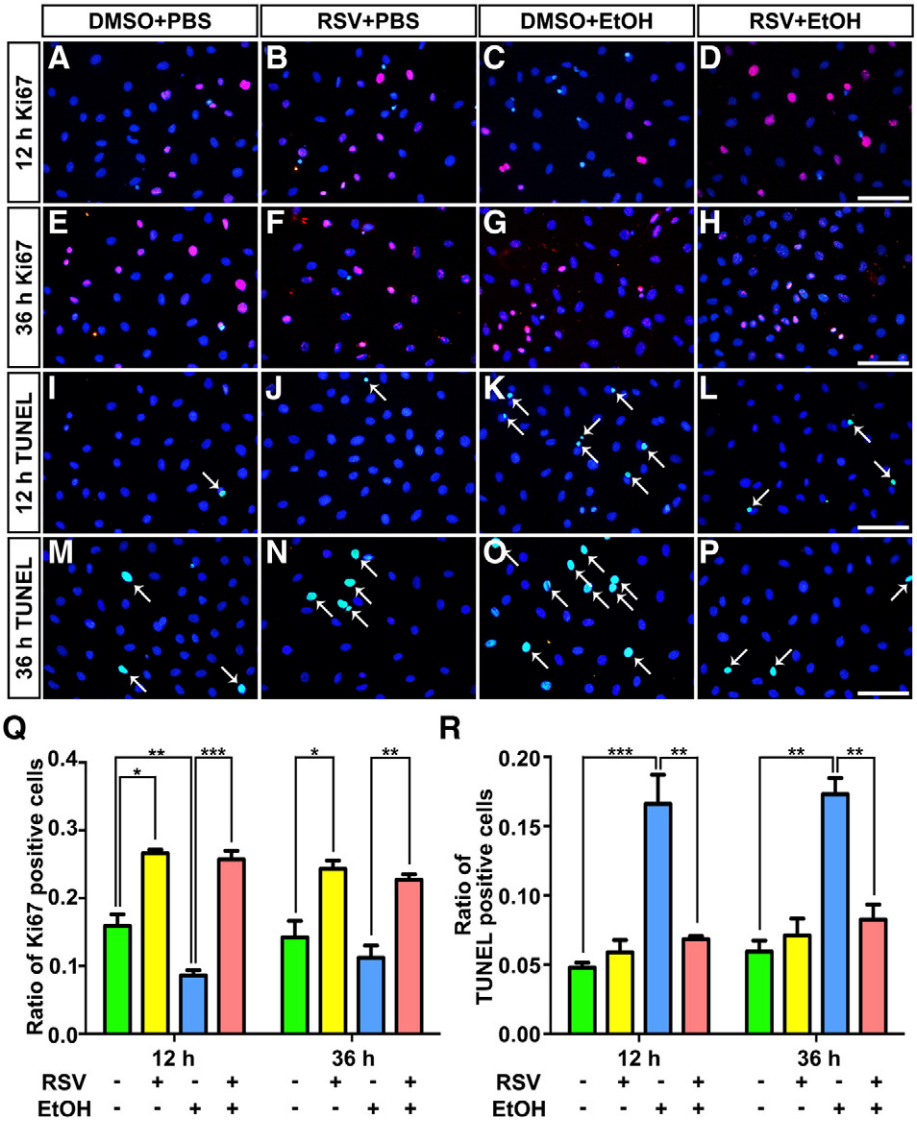

Fig. 10. Pretreatment with RSV rescues the EtOH-mediated proliferation decline and blocks the apoptosis of C17.2 neural precursor cells. (A–D, E–H) Representative images of C17.2 cells stained with Ki67 (red) and DAPI (blue) in EtOH exposure for 12 h and 36 h respectively. (Q) Statistical analysis of the ratio of Ki67-positive cells. (I–L, M–P) Representative images of C17.2 cells stained with TUNEL (green) and DAPI (blue). (R) Statistical analysis of the ratio of TUNEL-positive cells. Data are expressed as mean ± SEM. $^{*}p < 0.05$, $^{**}p < 0.01$, $^{***}p < 0.001$. Scale bars in $p = 50$ μm and applies to A–P.

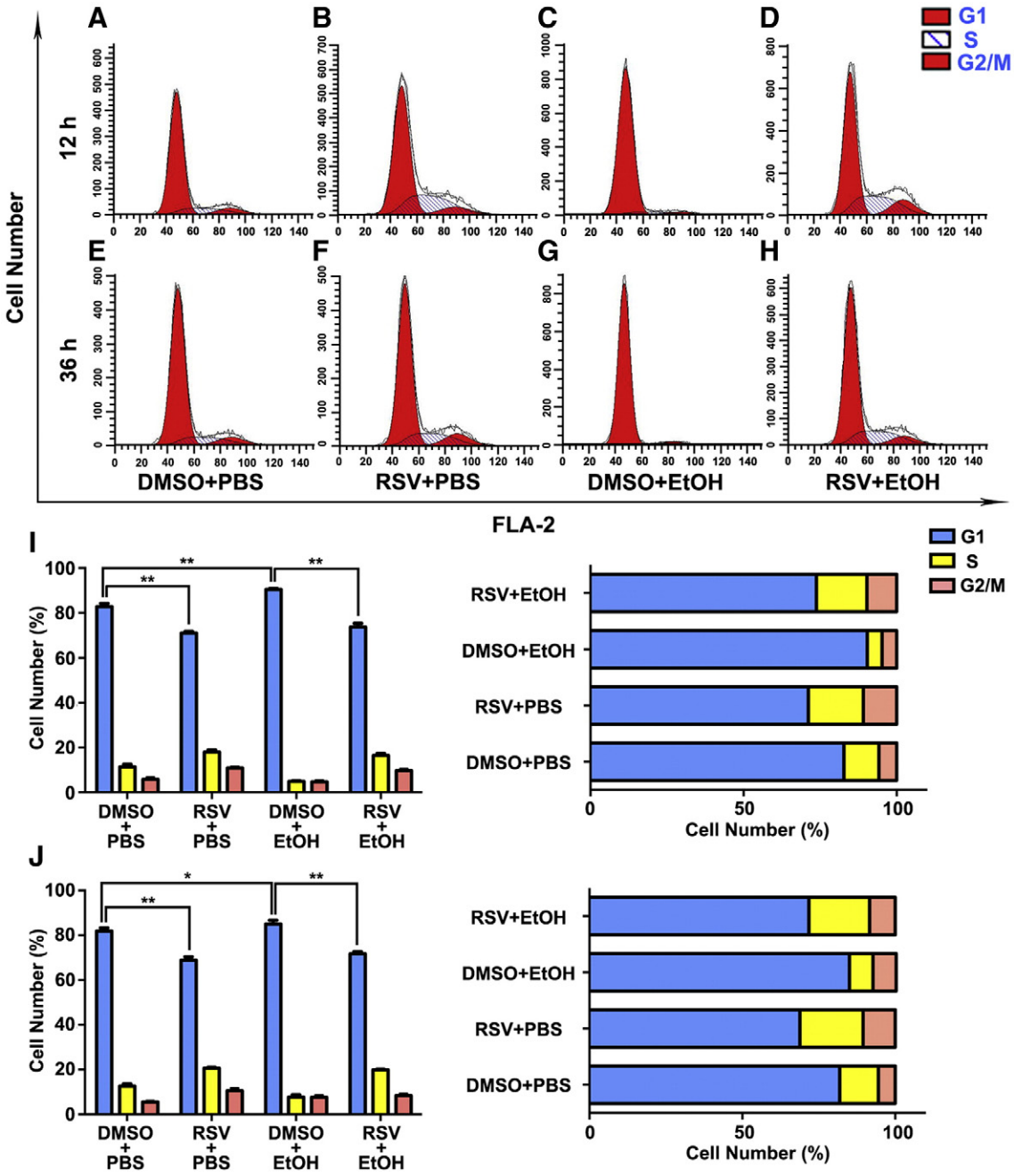

Fig. 11. Cell cycle analysis of C17.2 cells exposed to EtOH after pretreatment of RSV. (A–D, E–H) representative FACS analysis cell-cycle data after exposed to EtOH 12 h and 36 h respectively. (I, J) Statistical analysis of phases G1, S and G2/M in cell cycle analysis. Data are expressed as mean ± SEM. $^{*}p < 0.05$, $^{**}p < 0.01$.

4. Discussion

The present study demonstrated that administration of RSV significantly prevented the deleterious effects of EtOH on hippocampal neurogenesis and dendrite growth during the early postnatal period. In addition, RSV treatment also prevented the EtOH-induced reduction in the pool of NPCs in the DG. Furthermore, RSV treatment activated Sirt1 and reversed the down-regulated protein levels of hippocampal pERK and Hes1, which might be related to the proliferation and maintenance of NPCs [34,35].

The developing brain is extremely sensitive to EtOH neurotoxicity during the early postnatal period. Previous studies have demonstrated that EtOH administration to neonatal rats during this third trimester equivalent typically caused significant cell loss in the cerebellum, cerebral cortex, hippocampus and striatum [6,36]. Our results agree with these reports that EtOH administration at P7 reduced cell density in the DG [37], and RSV treatment reversed this effect. We further found that cell proliferation in the DG was also inhibited by EtOH, and RSV could reverse this effect.

A large body of evidence has been gathered to suggest that RGCs are transformed into NPCs in the postnatal DG and produce new granule neurons throughout life [38–41]. Exposure to EtOH in the developing brain induces RGC abnormalities that have been observed in humans and experimental animals [42–45]. EtOH also inhibits the proliferation and neurogenesis of human multipotent RGCs [46]. As these studies have indicated, EtOH exposure at P7 reduces the NPC pool in the DG [7,37], supporting our observation that EtOH reduces the RGC population that can differentiate into NPCs ($Nestin^{+}$/$BLBP^{+}$ or $GFAP^{+}$/$SOX2^{+}$).

Additionally, we also demonstrated that EtOH administration at P7 adversely affects the neuronal differentiation of newly generated cells as detected in the hippocampus at P14. All of these findings suggest that NPCs may be a target of EtOH-induced abnormalities in postnatal hippocampal development, and EtOH may thereby be involved in lifelong cognitive dysfunction by interfering with postnatal hippocampal neurogenesis [8,47].

RSV has been indicated in multiple roles in the CNS since its discovery [48–50]. Many discrepancies exist regarding the effects of RSV on hippocampus neurogenesis. Park et al. showed that RSV exhibits an inhibitory effect on hippocampal neurogenesis and cognitive function in adult mice [20]. However, other studies have observed that RSV promotes hippocampal neurogenesis and is beneficial for the recovery of cognitive dysfunction [22,51]. RSV function in hippocampal neurogenesis seems to be complicated and may be affected by many aspects, such as the dose of RSV, animal genotype and age and study duration. An important finding of our study is that RSV promotes hippocampal neurogenesis as demonstrated by increased BrdU incorporation and BLBP expression in the DG. Additionally, RSV can rescue defects in the pool of NPCs and neurogenesis in the DG abruptly caused by EtOH. Consistent with the findings from in vivo study, we further confirmed that EtOH reduced the mitogenic effects in the C17.2 cell line. RSV pretreatment effectively reversed the inhibition on NPC proliferation induced by EtOH.

Moreover, the EtOH-induced pathological alterations occurring in dendritic spines have attracted more attention because of the involvement of spine shape in learning and memory processes at the synaptic level [52–54]. In the present study, we noticed that EtOH exposure resulted in a reduction in spine density on granular neurons in the DG. Because a reduced number of dendritic spines seemed to reflect a reduction in total synapse number, the observed reductions in spine density might indicate early signs of synapse injury on granular neurons following EtOH exposure. Based on their morphological diversity, dendritic spines are usually divided into three categories [26,55], each of which endows different functional properties. Despite the difficulty in defining the precise function of each spine type, thin spines seem to be more plastic and are involved in learning, whereas mushroom spines play a larger role in memory [56–59]. Thus, the reduction in the fraction of mushroom spines and a marked increase in the proportion of stubby spines on granular neurons may contribute to EtOH-associated cognitive deficits. These observations are consistent with previous reports that prenatal EtOH exposure leads to developmental retardation in the maturation of dendritic spines and synapses [60–62]. Importantly, EtOH-induced pathological alterations occurring in dendritic spines could be rescued by RSV treatment. Most likely, the effects of RSV on dendrites may represent an efficient strategy to normalize cognitive deficits by neonatal intervention. Notably, the long unbranched processes of RGCs may convey signals to the nucleus that reflect the state of the local environment, thereby instructing the promotion of dendritic outgrowth in neurons [40]. Indeed, we observed that EtOH typically damaged RGCs in the GCL at P14, and this damage could be normalized by pretreatment with RSV. With these data combined, we may infer that RSV reverses or prevents EtOH-induced changes in spine density and dendritic components, and this effect may be partially related to its contribution to RGC maintenance.

Studies suggest that the altered ERK signaling pathway is involved in the regulation of NPC proliferation [63,64]. Acute EtOH exposure reduces ERK1/2 phosphorylation in the adolescent hippocampus associated with disruption of hippocampal-dependent memory acquisition [65]. In accordance with previous results, we found that EtOH decreased pERK/ERK levels in the hippocampus, and RSV treatment antagonized this reduction. These results indicated that the RSV-induced increase in pERK may be relevant to its effect on proliferation of NPCs in EtOH-treated mice. Hes1 is an essential effector in Notch signaling, which regulates the maintenance of RGCs [33,66]. The absence of the *Hes1* gene leads to a depletion of RGCs, a reduction in cell number and a lack of later-born neurons [67]. Decreased levels of Hes1 in EtOH-treated mice suggest that depletion of RGCs by EtOH may be related to the decreased NPC pool in the DG. A body of evidence has confirmed that RSV exerts neuroprotective actions through activation of Sirt1 [68,69]. Moreover, Sirt1 is involved in the self-renewal, multipotency, and fate determination of NPCs [70] In line with these studies, we observed that RSV pretreatment increased the Sirt1 level in the hippocampus after the EtOH exposure. This possibly inferred that Sirt1 activation by RSV might be involved in the reversed inhibition of pERK and Hes1 induced by EtOH exposure.

5. Conclusions

The present study demonstrates that the EtOH-induced reduction in hippocampal neurogenesis involves hippocampal pERK and Hes1 expressions during the early postnatal period. RSV activation of Sirt1 exhibits a neuroprotective effect against EtOH-induced decreases in neurogenesis in neonatal mice. RSV could thus open new avenues for preventing EtOH-mediated toxicity of the developing hippocampus.

Conflict of interest

The authors declare that they have no conflicts of interest.

Acknowledgments

This study was supported by the National Natural Science Foundation of China (no. 81371197 and no. 31271051) and the Natural Science Foundation Project of CQ CSTC (no. 2013jjB10028).

References

[1] S.K. Clarren, D.W. Smith, The fetal alcohol syndrome, N. Engl. J. Med. 298 (19) (1978) 1063–1067.
[2] C.E. Wood, Maternal binge drinking and fetal neuronal damage, Exp. Physiol. 92 (5) (2007) 821.
[3] M. Ungerer, J. Knezovich, M. Ramsay, In utero alcohol exposure, epigenetic changes, and their consequences, Alcohol. Res. 35 (1) (2013) 37–46.
[4] B.S. Basavarajappa, I. Ninan, O. Arancio, Acute ethanol suppresses glutamatergic neurotransmission through endocannabinoids in hippocampal neurons, J. Neurochem. 107 (4) (2008) 1001–1013.
[5] A.K. Singh, et al., In vitro neurogenesis from neural progenitor cells isolated from the hippocampus region of the brain of adult rats exposed to ethanol during early development through their alcohol-drinking mothers, Alcohol Alcohol. 44 (2) (2009) 185–198.
[6] D.J. Livy, et al., Fetal alcohol exposure and temporal vulnerability: effects of binge-like alcohol exposure on the developing rat hippocampus, Neurotoxicol. Teratol. 25 (4) (2003) 447–458.
[7] A. Ieraci, D.G. Herrera, Single alcohol exposure in early life damages hippocampal stem/progenitor cells and reduces adult neurogenesis, Neurobiol. Dis. 26 (3) (2007) 597–605.
[8] G.F. Hamilton, et al., Neonatal alcohol exposure disrupts hippocampal neurogenesis and contextual fear conditioning in adult rats, Brain Res. 1412 (2011) 88–101.
[9] S. Temple, A. Alvarez-Buylla, Stem cells in the adult mammalian central nervous system, Curr. Opin. Neurobiol. 9 (1) (1999) 135–141.
[10] A.R. Schlessinger, W.M. Cowan, D.I. Gottlieb, An autoradiographic study of the time of origin and the pattern of granule cell migration in the dentate gyrus of the rat, J. Comp. Neurol. 159 (2) (1975) 149–175.
[11] M.A. Taffe, et al., Long-lasting reduction in hippocampal neurogenesis by alcohol consumption in adolescent nonhuman primates, Proc. Natl. Acad. Sci. U. S. A. 107 (24) (2010) 11104–11109.
[12] R.F. Berman, J.H. Hannigan, Effects of prenatal alcohol exposure on the hippocampus: spatial behavior, electrophysiology, and neuroanatomy, Hippocampus 10 (1) (2000) 94–110.
[13] B.D. Gehm, et al., Resveratrol, a polyphenolic compound found in grapes and wine, is an agonist for the estrogen receptor, Proc. Natl. Acad. Sci. U. S. A. 94 (25) (1997) 14138–14143.
[14] M. Sovak, Grape extract, resveratrol, and its analogs: a review, J. Med. Food 4 (2) (2001) 93–105.
[15] S. Yousuf, et al., Resveratrol exerts its neuroprotective effect by modulating mitochondrial dysfunctions and associated cell death during cerebral ischemia, Brain Res. 1250 (2009) 242–253.
[16] C. Menard, S. Bastianetto, R. Quirion, Neuroprotective effects of resveratrol and epigallocatechin gallate polyphenols are mediated by the activation of protein kinase C gamma, Front. Cell. Neurosci. 7 (2013) 281.

[17] O. Ates, et al., Neuroprotection by resveratrol against traumatic brain injury in rats, Mol. Cell. Biochem. 294 (1–2) (2007) 137–144.
[18] U. Sonmez, et al., Neuroprotective effects of resveratrol against traumatic brain injury in immature rats, Neurosci. Lett. 420 (2) (2007) 133–137.
[19] J. Moriya, et al., Resveratrol improves hippocampal atrophy in chronic fatigue mice by enhancing neurogenesis and inhibiting apoptosis of granular cells, Biol. Pharm. Bull. 34 (3) (2011) 354–359.
[20] H.R. Park, et al., Resveratrol inhibits the proliferation of neural progenitor cells and hippocampal neurogenesis, J. Biol. Chem. 287 (51) (2012) 42588–42600.
[21] T. West, M. Atzeva, D.M. Holtzman, Pomegranate polyphenols and resveratrol protect the neonatal brain against hypoxic–ischemic injury, Dev. Neurosci. 29 (4–5) (2007) 363–372.
[22] S. Madhyastha, S. Sekhar, G. Rao, Resveratrol improves postnatal hippocampal neurogenesis and brain derived neurotrophic factor in prenatally stressed rats, Int. J. Dev. Neurosci. 31 (7) (2013) 580–585.
[23] L.S. Steelman, et al., JAK/STAT, Raf/MEK/ERK, PI3K/Akt and BCR-ABL in cell cycle progression and leukemogenesis, Leukemia 18 (2) (2004) 189–218.
[24] T. Ohtsuka, et al., Roles of the basic helix–loop–helix genes Hes1 and Hes5 in expansion of neural stem cells of the developing brain, J. Biol. Chem. 276 (32) (2001) 30467–30474.
[25] Y. Yang, et al., Activation of liver X receptor is protective against ethanol-induced developmental impairment of Bergmann glia and Purkinje neurons in the mouse cerebellum, Mol. Neurobiol. 49 (1) (2014) 176–186.
[26] A. Chakraborti, et al., Cranial irradiation alters dendritic spine density and morphology in the hippocampus, Plos One 7 (7) (2012) e40844.
[27] X. Chen, et al., Sodium iodate influences the apoptosis, proliferation and differentiation potential of radial glial cells in vitro, Cell. Physiol. Biochem. 34 (4) (2014) 1109–1124.
[28] S.J. Wang, et al., Effect of optogenetic stimulus on the proliferation and cell cycle progression of neural stem cells, J Membr Biol 247 (6) (2014) 493–500.
[29] J. Huang, et al., Propofol administration during early postnatal life suppresses hippocampal neurogenesis, Mol. Neurobiol. (2015) (Epub Jan. 11, 2015).
[30] L.H. Pevny, S.K. Nicolis, Sox2 roles in neural stem cells, Int. J. Biochem. Cell Biol. 42 (3) (2010) 421–424.
[31] S. Subbanna, et al., Anandamide-CB1 receptor signaling contributes to postnatal ethanol-induced neonatal neurodegeneration, adult synaptic, and memory deficits, J. Neurosci. 33 (15) (2013) 6350–6366.
[32] S.L. Samudio-Ruiz, et al., Prenatal ethanol exposure persistently impairs NMDA receptor-dependent activation of extracellular signal-regulated kinase in the mouse dentate gyrus, J. Neurochem. 109 (5) (2009) 1311–1323.
[33] S. Kamakura, et al., Hes binding to STAT3 mediates crosstalk between Notch and JAK–STAT signalling, Nat. Cell Biol. 6 (6) (2004) 547–554.
[34] N.M. Fournier, et al., Vascular endothelial growth factor regulates adult hippocampal cell proliferation through MEK/ERK- and PI3K/Akt-dependent signaling, Neuropharmacology 63 (4) (2012) 642–652.
[35] H. Shimojo, T. Ohtsuka, R. Kageyama, Oscillations in notch signaling regulate maintenance of neural progenitors, Neuron 58 (1) (2008) 52–64.
[36] D.J. Bonthius, J.R. West, Alcohol-induced neuronal loss in developing rats: increased brain damage with binge exposure, Alcohol. Clin. Exp. Res. 14 (1) (1990) 107–118.
[37] L.G. Coleman Jr, et al., Postnatal day 7 ethanol treatment causes persistent reductions in adult mouse brain volume and cortical neurons with sex specific effects on neurogenesis, Alcohol 46 (6) (2012) 603–612.
[38] M.F. Eckenhoff, P. Rakic, Radial organization of the hippocampal dentate gyrus: a Golgi, ultrastructural, and immunocytochemical analysis in the developing rhesus monkey, J. Comp. Neurol. 223 (1) (1984) 1–21.
[39] M. Rickmann, D.G. Amaral, W.M. Cowan, Organization of radial glial cells during the development of the rat dentate gyrus, J. Comp. Neurol. 264 (4) (1987) 449–479.
[40] B. Brunne, et al., Origin, maturation, and astroglial transformation of secondary radial glial cells in the developing dentate gyrus, Glia 58 (13) (2010) 1553–1569.
[41] L. Xu, et al., Radial glia, the keystone of the development of the hippocampal dentate gyrus, Mol. Neurobiol. 51 (1) (2014) 131–141.
[42] S. Valles, et al., Glial fibrillary acidic protein expression in rat brain and in radial glia culture is delayed by prenatal ethanol exposure, J. Neurochem. 67 (6) (1996) 2425–2433.
[43] S. Komatsu, et al., Prenatal exposure to ethanol induces leptomeningeal heterotopia in the cerebral cortex of the rat fetus, Acta Neuropathol. 101 (1) (2001) 22–26.
[44] S.M. Mooney, J.A. Siegenthaler, M.W. Miller, Ethanol induces heterotopias in organotypic cultures of rat cerebral cortex, Cereb. Cortex 14 (10) (2004) 1071–1080.
[45] G. Rubert, et al., Ethanol exposure during embryogenesis decreases the radial glial progenitor pool and affects the generation of neurons and astrocytes, J. Neurosci. Res. 84 (3) (2006) 483–496.
[46] Z. Mo, V. Milivojevic, N. Zecevic, Enforced Pax6 expression rescues alcohol-induced defects of neuronal differentiation in cultures of human cortical progenitor cells, Alcohol. Clin. Exp. Res. 36 (8) (2012) 1374–1384.
[47] J. Zou, F.T. Crew, Inflammasome-IL-1β signaling mediates ethonal inhibition of hippocampal neurogenesis, Front. Neurosci. 6 (2012) 77.
[48] F. Zhang, J. Liu, J.S. Shi, Anti-inflammatory activities of resveratrol in the brain: role of resveratrol in microglial activation, Eur. J. Pharmacol. 636 (1–3) (2010) 1–7.
[49] A. Quincozes-Santos, C. Gottfried, Resveratrol modulates astroglial functions: neuroprotective hypothesis, Ann. N. Y. Acad. Sci. 1215 (2011) 72–78.
[50] N. Singh, M. Agrawal, S. Dore, Neuroprotective properties and mechanisms of resveratrol in in vitro and in vivo experimental cerebral stroke models, ACS Chem. Neurosci. 4 (8) (2013) 1151–1162.
[51] N. Harada, et al., Resveratrol improves cognitive function in mice by increasing production of insulin-like growth factor-I in the hippocampus, J. Nutr. Biochem. 22 (12) (2011) 1150–1159.
[52] I. Morgado-Bernal, Learning and memory consolidation: linking molecular and behavioral data, Neuroscience 176 (2011) 12–19.
[53] M. Patterson, R. Yasuda, Signalling pathways underlying structural plasticity of dendritic spines, Br. J. Pharmacol. 163 (8) (2011) 1626–1638.
[54] M. Bosch, Y. Hayashi, Structural plasticity of dendritic spines, Curr. Opin. Neurobiol. 22 (3) (2012) 383–388.
[55] A. Peters, I.R. Kaiserman-Abramof, The small pyramidal neuron of the rat cerebral cortex. The perikaryon, dendrites and spines, Am. J. Anat. 127 (4) (1970) 321–355.
[56] K.M. Harris, F.E. Jensen, B. Tsao, Three-dimensional structure of dendritic spines and synapses in rat hippocampus (CA1) at postnatal day 15 and adult ages: implications for the maturation of synaptic physiology and long-term potentiation, J. Neurosci. 12 (7) (1992) 2685–2705.
[57] J. Spacek, K.M. Harris, Three-dimensional organization of smooth endoplasmic reticulum in hippocampal CA1 dendrites and dendritic spines of the immature and mature rat, J. Neurosci. 17 (1) (1997) 190–203.
[58] Z. Parnass, A. Tashiro, R. Yuste, Analysis of spine morphological plasticity in developing hippocampal pyramidal neurons, Hippocampus 10 (5) (2000) 561–568.
[59] J. Bourne, K.M. Harris, Do thin spines learn to be mushroom spines that remember? Curr. Opin. Neurobiol. 17 (3) (2007) 381–386.
[60] J.P. Rice, et al., Effects of exposure to moderate levels of ethanol during prenatal brain development on dendritic length, branching, and spine density in the nucleus accumbens and dorsal striatum of adult rats, Alcohol 46 (6) (2012) 577–584.
[61] C.L. Cullen, et al., Low dose prenatal ethanol exposure induces anxiety-like behaviour and alters dendritic morphology in the basolateral amygdala of rat offspring, PLoS One 8 (1) (2013) e54924.
[62] A.M. Romero, et al., Chronic alcohol alters dendritic spine development in neurons in primary culture, Neurotox. Res. 24 (4) (2013) 532–548.
[63] Y.L. Hao, et al., Mood stabilizer valproate promotes ERK pathway-dependent cortical neuronal growth and neurogenesis, J. Neurosci. 24 (29) (2004) 6590–6599.
[64] J. Hsieh, et al., Histone deacetylase inhibition-mediated neuronal differentiation of multipotent adult neural progenitor cells, Proc. Natl. Acad. Sci. U. S. A. 101 (47) (2004) 16659–16664.
[65] M. Spanos, J. Besheer, C.W. Hodge, Increased sensitivity to alcohol induced changes in ERK Map kinase phosphorylation and memory disruption in adolescent as compared to adult C57BL/6J mice, Behav. Brain Res. 230 (1) (2012) 158–166.
[66] B.R. Nelson, et al., Dynamic interactions between intermediate neurogenic progenitors and radial glia in embryonic mouse neocortex: potential role in Dll1-notch signaling, J. Neurosci. 33 (21) (2013) 9122–9139.
[67] J. Hatakeyama, et al., Hes genes regulate size, shape and histogenesis of the nervous system by control of the timing of neural stem cell differentiation, Development 131 (22) (2004) 5539–5550.
[68] G. Ramadori, et al., Brain SIRT1: anatomical distribution and regulation by energy availability, J. Neurosci. 28 (40) (2008) 9989–9996.
[69] G.M. Pasinetti, et al., Roles of resveratrol and other grape-derived polyphenols in Alzheimer's disease prevention and treatment, Biochim. Biophys. Acta 1852 (6) (2015) 1202–1208.
[70] L. Tiberi, et al., BCL6 controls neurogenesis through Sirt1-dependent epigenetic repression of selective Notch targets, Nat. Neurosci. 12 (2012) 1627–1635.